An Overlooked Silica Source of the Modern Oceans: Are Sandy Beaches the Key?

Sébastien Fabre[1]*, Catherine Jeandel[2]*, Thomas Zambardi[2], Michel Roustan[3] and Rafaël Almar[2]

[1] UMR 5277 Institut de Recherche en Astrophysique et Planétologie, Université de Toulouse, CNRS, CNES, Université Paul Sabatier, Toulouse, France, [2] UMR 5566 Laboratoire d'Études en Géophysique et Océanographie Spatiales, Université de Toulouse, CNRS, IRD, CNES, Université Paul Sabatier, Toulouse, France, [3] Institut National des Sciences Appliquées de Toulouse, Université de Toulouse, Toulouse, France

We consider the Si flux resulting from sand grain dissolution on beaches under the pressure of the intensive and continuous shaking by the waves, a potential source of oceanic DSi that is not currently considered. Today, DSi source and sink fluxes are balanced within large uncertainties, at ca. 10.4 ± 4.2 and $14.6 \pm 7.8 \times 10^{12}$ mol yr^{-1}, respectively, underlining that some processes are not well constrained and possibly overlooked so far. To quantitatively explore this idea, we first realized an experimental dissolution of quartz grains in a stirred vessel designed to simulate the sediment orbital motion induced by the waves. These experiments lead to the calculation of a solid–liquid mass-transfer coefficient directly linked to the rotation speed of the shaker. This coefficient being itself related to the energy communicated to the liquid, we could apply the Nienow relationship to calculate a mass-transfer coefficient for beach sand exposed to 1 m height waves. Extrapolation of this value to the whole sandy beaches led us to conclude that this mechanism could be significant, shortening the calculated residence time of oceanic DSi by up to a factor 2.

Keywords: silica, quartz, weathering, beaches, ocean chemistry

INTRODUCTION

Since the end of the 20th century, the understanding and the importance of the silicon cycle in marine biogeochemistry have increased, because of the need to constrain the role of diatoms and siliceous species in the export of carbon toward the deep ocean (Tréguer and De La Rocha, 2013).

Recent reviews (Tréguer and De La Rocha, 2013; Frings et al., 2016; Rahman et al., 2019) proposes an overview of the global ocean silica cycle comprising inputs (e.g., dissolved riverine, aeolian dusts, and hydrothermal fluids) and outputs (e.g., sedimentation of biogenic particles on coastal margins followed by reverse weathering and opal burial in the abyss) assumed to be at steady state, fluxes being expressed in 10^{12} mol yr^{-1}. It is worth noting that some of these fluxes were defined to close the ocean mass-balance, and are poorly constrained by independent evidence. Indeed, despite numerous work (e.g., DeMaster, 1981; De La Rocha and Bickle, 2005; Ragueneau et al., 2006; Rahman et al., 2017) major uncertainties remain concerning the magnitudes of these fluxes (Ragueneau et al., 2000; Rahman et al., 2017). As previously noticed by Tréguer and De La Rocha (2013), the flux of particulate silica (lithogenic and biogenic) to estuaries calculated by Dürr et al. (2011) is 147 ± 44 Tmol Si yr^{-1}. How much of this flux actually dissolves remains unknown. In addition, while Rahman et al. (2019) revisited the importance

of the reverse weathering in deltaic environments, other recent studies strongly suggest that the release of chemical species from solid material deposited at the land–ocean interface are occurring (Jeandel and Oelkers, 2015). Field, laboratory, and modeling works suggest that these fluxes are considerable, although less than a few percent of the sediment dissolves (Lacan and Jeandel, 2005; Arsouze et al., 2009). Jeandel (2016) underlined that the environments where such processes take place can be very diverse, from deep margins to subsurface coastal submarine groundwater discharge and that the release mechanisms have to be better quantified and constrained. Among others, roughly one-third of the world's shorelines are made of sand beaches (Brown and Mclachlan, 2002; Luijendijk et al., 2018), in other words huge resources of silicates. Here, we assess the impact of wave energy in the beach surf zone on the dissolution of quartz sand supplied by weathering. We propose that a key input term to DSi could have been neglected in current estimates of the oceanic Si budget: abiotic dissolution of quartz grains mediated in the surf zone where waves break.

Quartz dissolution has been extensively studied despite the challenges in measuring its dissolution rate which is generally slow (Knauss and Wolery, 1988; Brady and Walther, 1990; Bennett, 1991; Dove, 1994; Gautier et al., 2001).

Recent studies of Crundwell (2014) tentatively gathered all the literature data in a single model of dissolution for all the silicates. The rate of silicate dissolution proposed follows the equation:

$$\text{rate} = k[c]^n \exp(-E_A/RT)A(1 - Q/K) \tag{1}$$

where $[c]$ represents the activity or concentration of a reactant, k the rate constant $[\text{mol}(\text{mol/m}^3)^{-n}/(\text{m}^2\ \text{s})]$, n the order of the reaction, E_A the activation energy (kJ/mol), R the gas constant (kJ/mol/K), and T the temperature (K). A is the specific surface area (m^2) and $(1-Q/K)$ the chemical affinity. Rates are expressed in mol s^{-1}.

Measured quartz dissolution rates at 25°C suggest that (i) quartz dissolves under both acidic and alkaline pH conditions and (ii) the order of the reaction is 0.5 with respect to H^+ or OH^- (Casey, 1991; Brantley et al., 2008). These dissolution models consider static solutions, where mass transport is much slower than the chemical dissolution reaction. Such reactions are named "transport controlled reactions." Contrastingly, when a mineral dissolves in a mobile solvent, the measured rate derives from a combination of the rate of chemical reaction at the solid–liquid interface (pure dissolution) and the diffusion velocity across the diffusional boundary layer in the vicinity of the interface when placed in a flow (mass transport). The mechanism proposed here will show that diffusion is no longer a limiting step of quartz dissolution under more dynamic mechanical conditions in the surf zone. Earlier studies conducted *in situ* and *ex situ* on bottom sediment dissolution in seawater (e.g., Gehlen et al., 1995; Van Cappellen, 1996) showed that this could be an important Si input term. However, these studies were made on biogenic silica while we are focusing here on the lithogenic phase.
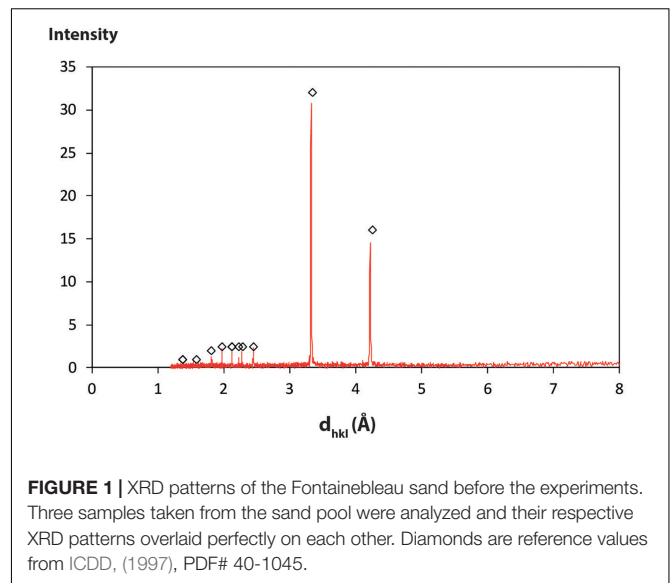

FIGURE 1 | XRD patterns of the Fontainebleau sand before the experiments. Three samples taken from the sand pool were analyzed and their respective XRD patterns overlaid perfectly on each other. Diamonds are reference values from ICDD, (1997), PDF# 40-1045.

METHODOLOGY

Nature and Origin of the Samples

The sediments selected for this study were quartz grains from the sand of Fontainebleau formation (France). The Fontainebleau sandstone is an early Oligocene (36–27 My) unit, 50–80 m thick, made of fine grained, well-sorted, quartz arenite.

This sediment is thought to be representative of the abiotic material present in sandy beaches. Indeed, fine sand grain size (namely 125–250 μm) represents the most abundant feature – circa 10^6 km^2 – of alluvial and coastal depositional systems (Haddad et al., 2006).

Materials and Methods
Sample Properties

Polarizing microscope observation did not show any mineral phases other than quartz in the sample and X-ray diffraction (XRD) revealed only α-quartz diffraction peaks. Grain size distribution obtained by laser diffraction (Coulter LS100 Q) indicated a very sharp unimodal symmetrical distribution with a geometric mean of 270 μm (Orton and Reading, 1993).

X-ray diffraction analyses of the initial sand powder were performed on a Bruker® D8 XRD diffractometer (CuKα1 + 2 radiation) over the 2–60° 2Θ angular range with 0.02° 2Θ steps and 2 s per step. It confirmed that the sand was only composed of pure α-quartz (**Figure 1**). Its homogeneity was checked by performing XRD analysis of three different samples, leading to three undistinguishable XRD patterns. No particular preparation was carried out on the samples in order to maintain their surface state as close as possible to that of natural quartz grains.

Experimental Protocol

For each experiment, sand and deionized water or filtered commercial abiotic seawater[1] (pH ≈ 7.85 at 20°C) with various

---

[1]Surface seawater was collected unfiltered from the North Atlantic Ocean and transported in large containers to the Ocean Scientific International Limited

rock–water ratios (R/W) were introduced into HDPE closed containers and placed on an agitator (Stuart, Orbital Shaker; see **Table 1** for a summary of the experimental conditions). A first set of experiments was conducted for 10 days under static or dynamic conditions (0, 80, or 230 rotations per minute, rpm). At various time intervals, aliquots of 5 mL were sampled, filtered (0.22 μm mesh), and analyzed. The final sampled solution represented <10% of the initial volume. A second set of experiments with variable rock/water ratio – from 0.18 to 1.25 — was conducted during 270 h (≈11 days) with a constant rotation speed (230 rpm). All the experiments were performed at room temperature (21°C).

Solution Analyses

pH was measured at room temperature with a WRW IS 60 pH-meter coupled to an Orion electrode, previously calibrated at pH 4 and 7. The aqueous silica concentration was measured using the molybdate method (Strickland and Parsons, 1972) with a Technicon Analyzer II Colorimeter. Seawater dissolved Si analysis rigorously followed international protocols (Hood et al., 2010). Replicate measurements were performed establishing that the precision of the measurements is 1.78 μmol L^{-1} and blanks are negligible.

---

laboratory (Havant, United Kingdom). The seawater samples were then filtered through 2.0 and 0.2 μm cartridge filters, sterilized by ultraviolet irradiation and mixed with de-ionized water to adjust the salinity close to 35‰. The sample material was stored in pre-cleaned borosilicate bottles. Conductivity calibration was carried out using a KCl solution of known salt concentration, whereby the linear correlation between conductivity and concentration permitted the IAPSO seawater RM conductivity ratio (K15) to be determined. The IAPSO seawater that was used in this study belonged to batch P150 made on 22 May 2008 with a K15 equal to 0.99978 and a salinity of 34.991.

TABLE 1 | Recap chart of the experimental conditions.

First set of experiments: influence of the rotation speed

Seawater	
Water (g)	300
Sand (g)	170
R/W	0.55
Rotation speed (rpm)	230, 80, static
Duration (h)	240
Freshwater	
Water mass	300
Sand mass	170
R/W	0.55
Rotation speed (rpm)	230, 80, static
Duration (h)	270

Second set of experiments: influence of the water/rock ratio

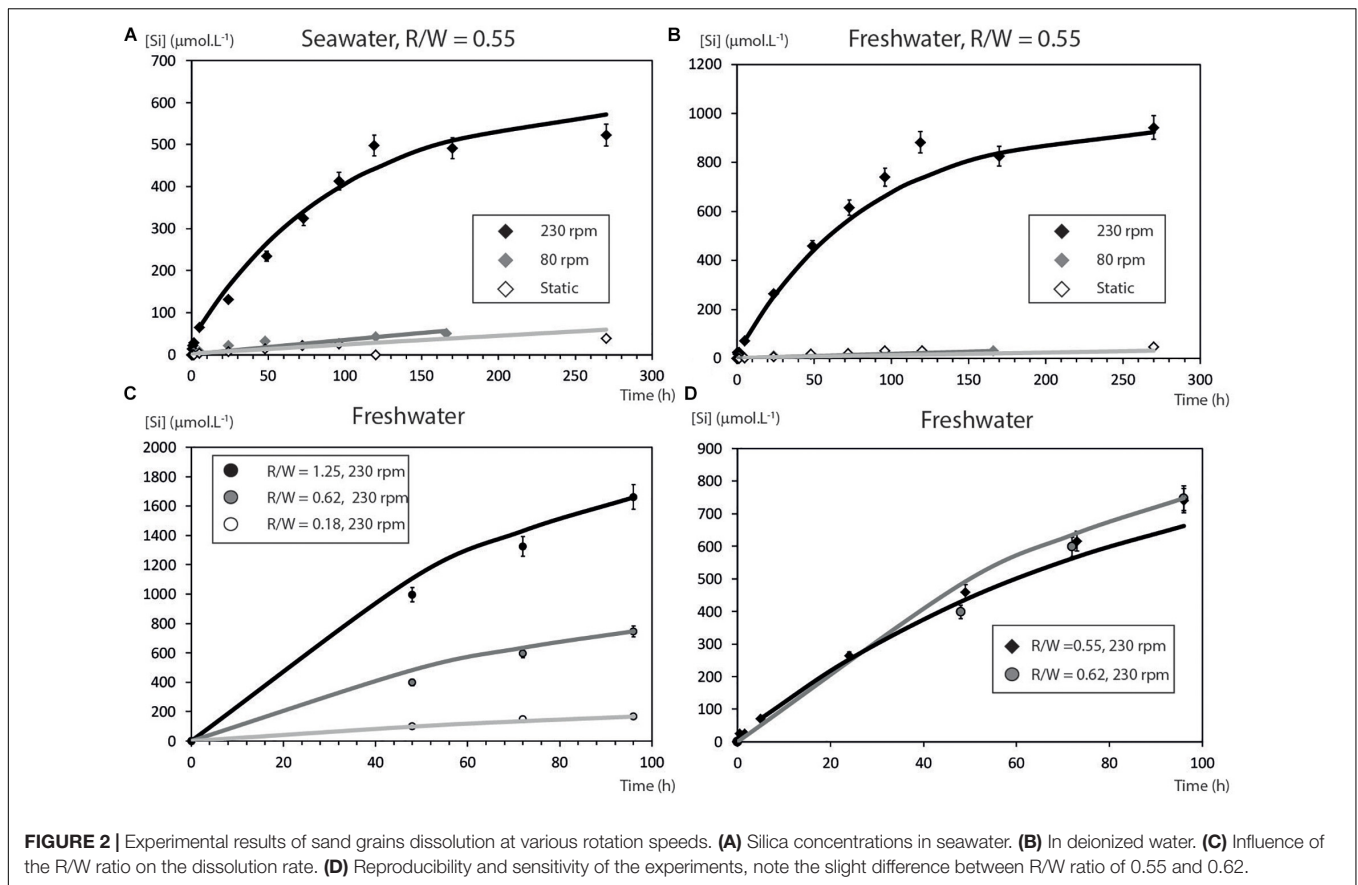| Freshwater			
Water mass (g)	320	144	70
Sand mass (g)	60	90	90
R/W	0.18	0.62	1.25
Rotation speed (rpm)	230	230	230
Duration (h)	240	240	240

EXPERIMENTS

Results

Rates of Dissolution

Figures 2A,B depict the experimental data expressed as silica concentration as a function of time (**Table 2**). Not surprisingly, in static mode, quartz dissolution is very slow. However, silica concentration increases modestly when mixing at 85 rpm and far more significantly at 230 rpm to reach a value of 523 μmol L^{-1} in seawater and ≈943 μmol L^{-1} in fresh water. From a kinetic point of view, after a rapid initial burst, the rate of dissolution decreases with time to reach a plateau when the solution approaches saturation relative to quartz. Other experiments using higher rotation speeds (330 rpm) – not depicted[2] – show no significant increase of silica concentration. Saturation indices $SI = \log\left(\frac{Q}{K(T)}\right)$, where Q is the ionic activity product and $K(T)$ the reaction equilibrium constant were calculated for three Si bearing phases (namely Quartz, Chalcedony, and Amorphous silica) using PHREEQC software (Parkhurst and Appelo, 1999) coupled to the Lawrence Livermore National Laboratory (LLNL) database (Delaney and Wolery, 1989; **Table 3**). Using these values we find that experimental solutions stayed under-saturated for all the considered phases in static mode and for low rotation speed whatever the media. At 230 rpm, however, solutions became over-saturated for quartz and chalcedony between 1440 and 2940 h, while dissolution was still operating for several hours before reaching the plateau phase. This means that agitation maintains dissolution of quartz grains even under solution chemical conditions thermodynamically unfavorable. Filtering to 0.22 μm ensured that we measured only dissolved silica. We are aware of the fact that the molybdate method will detect the monomeric SiO$_2$ only. However, as noticed by Ning (2003) colloidal silica is depolymerized by seawater, meaning that in the analyzed seawater SiO$_2$ is in the monomeric form only.

Variation of the rock–water ratio clearly illustrates the proportionality between the amount of quartz grains and dissolved Si concentrations (**Figure 2D**), which is easy to understand on a qualitative point of view: as rock/water ratio diminishes the DSi concentration lowers by dilution. This point is discussed quantitatively in the section "Chemical Modeling." In order to test the reproducibility and the sensitivity of the experiments to the R/W ratio, two others experiments with very close R/W ratios were performed (**Figure 2D**). The DSi concentrations values are not significantly different except for the middle value.

The effect of organic coatings on quartz dissolution was not considered in our experimental setup because we were focusing on the abiotic dissolution only. However, organic coatings could modify the quartz dissolution in two opposite ways. On the one hand, organic acids at circum neutral pH accelerate the quartz dissolution and enhance its solubility in seawater (Bennett, 1991). On the other hand, organic coatings

---

[2]The experiments were only performed to reach the final value – after 270 h of experiment. The silica concentration is 0.016 g/L (569 μmol/L) for seawater and 0.028 g/L (996 μmol/L). for fresh water.

FIGURE 2 | Experimental results of sand grains dissolution at various rotation speeds. **(A)** Silica concentrations in seawater. **(B)** In deionized water. **(C)** Influence of the R/W ratio on the dissolution rate. **(D)** Reproducibility and sensitivity of the experiments, note the slight difference between R/W ratio of 0.55 and 0.62.

deposited onto the silica surface can decrease the dissolution rate by restricting access to reactive surface area (Banfield et al., 1997). Contrastingly, however, Van Cappellen and Qiu (1997) showed that the formation of protective organic coatings do not explain the observed reduction in biogenic silica reactivity. These observations underline that the role of organic coatings on quartz dissolution requires more investigation, while Brantley et al. (2008) underlined that inorganic controls on dissolution such as Al sorption could affect more the quartz dissolution rate than organic coating.

Evolution of Quartz Grain Morphology During Dissolution

The evolution of grain surfaces was observed using Scanning Electron Microscopy (**Figure 3**). Neither grain rounding nor etch pit formation was apparent on the micrographs, although more discrete features could be observed. Worn blocky conchoidal fracture patterns can be seen in **Figure 2A**, fresher breakage patterns, probably produced by grinding of the other grains are visible in **Figure 2B**. Old slightly curved grooves or scratches measuring t 5–15 μ in length are shown in **Figure 3C**. On reacted grain surfaces (**Figure 3D**) V-shaped indentations and friction marks are visible. These latter features are likely caused by contact between sharp edges of one sand grain and another. Finally, worn etch pits of the initial grains with rounded edges are different from oriented V-shaped patterns on final quartz grain surfaces. They probably result from chemical etching in seawater

(Krinsley and Margolis, 1969) but all these features pre-exist to the experiments as previously noted by Vos et al. (2014). The possibility that dissolution of quartz cement could result in the kinetic observed can be ruled out for two reasons: (1) Haddad et al. (2006) showed that the very small fraction of cement in the studied sand is mostly constituted of crystallized quartz and (2) our SEM observations confirmed these findings (**Figure 3**).

Chemical Modeling

Attempts to model the experiments using Eq. (1) failed because of its inappropriate formalism to describe grain dissolution in an agitated medium. Indeed, the diffusive contribution to quartz dissolution is no longer the limiting step. Forced convection is intense enough to maintain the chemical potential disequilibrium between the surface mineral and the solution. We therefore choose to use a shrinking sphere model to fit the experimental data, widely used in pharmaceutical and metallurgical domains even if the reactive surface area of grains did not significantly vary during the experiments (**Figure 3**). In such model, a simple Si mass balance equation between the grains and the solution is considered. Our approach was to assume a quasi-stationary mode, the particle dissolves faster in an agitated media because the boundary layer where the transport of aqueous species is driven by diffusion – slower than advection – is very thin. As a consequence, the difference between the Si concentration at the particle surface and at the end of the boundary limit – i.e.,

TABLE 2 | Experimental results.

First set of experiments

Seawater, R/W 0.55

230 rpm

Time (h)	0	0.5	1	1.5	5	24	49	73	96	119	170	270
[Si] (μmol/L^{-1})	0	14	21	28	64	132	235	324	413	498	491	523

85 rpm

Time (h)	0	0.5	1	1.5	5	24	48	120	166			
[Si] (μmol/L^{-1})	0	1	2	4	7	21	32	43	50			

No agitation

Time (h)	0	0.5	1	1.5	5	24	48	72	96	120	270	
[Si] (μmol/L^{-1})	0	0	0	0	4	7	14	21	25	25	39	

MQ water, R/W 0.55

230 rpm

Time (h)	0	0.5	1	1.5	5	24	49	73	96	119	170	270
[Si] (μmol/L^{-1})	0	25	18	25	71	263	459	616	740	883	826	943

85 rpm

Time (h)	0	0.5	1	1.5	5	24	48	120	166			
[Si] (μmol/L^{-1})	0	1	1	1	4	11	18	28	32			

No agitation

Time (h)	0	0.5	1	1.5	5	24	48	72	96	120	270	
[Si] (μmol/L^{-1})	0	0	0	0	4	7	18	21	32	32	46	

Second set of experiments

MQ water, R/W = 0.62

Time (h)	0	48	72	96
[Si] (μmol/L^{-1})	0	399	598	747

MQ water, R/W = 0.18

Time (h)	0	48	72	96
[Si] (μmol/L^{-1})	0	100	149	167

MQ water, R/W = 1.25

Time (h)	0	48	72	96
[Si] (μmol/L^{-1})	0	996	1324	1662

concentration gradient – is considered constant. As justified in detail in the **Supplementary Material**, the quantity of a given element transferred from the solid to the fluid can be expressed as:

$$F = kS(C_1 - C_2) \quad (2)$$

with F (mol s^{-1}) the mass flux,
k (m s^{-1}) the mass-transfer coefficient,
S (m^2) the grain surface area,
C_1 and C_2 (mol m^{-3}) are, respectively, concentrations in the solid and in the solution.

The quasi-stationary particle dissolution can be described by a mass balance between the amount of quartz grains dissolved and the increase in Si in solution for a time interval dt expressed as:

$$\frac{dC}{dt} = \frac{kS(t)}{V}(C^* - C) \quad (3)$$

with
V (m^3) reactor volume,
$S(t)$ (m^2) exchange surface area according to time,
C^* (kg m^{-3}) the maximum solid concentration in solution
C (kg m^{-3}) solid concentration.

The mass transfer coefficient (k) was obtained by fitting Eq. (3) to the experimental data for the best test conditions (**Figure 2B**). Mean values and standard deviation of the different measurements are reported in **Tables 4**, **5**. The data fitting is very good in all the cases (**Tables 4**, **5**, sum of quadratic error $< 10^{-5}$). The very good agreement of the fit (**Figure 2** and **Table 2**) argues in favor of the dissolution model described before. One can notice that k values are low compared to other materials which are circa 10^{-4} m s^{-1} (Roustan, 2003).

As rotation speed increases, k increases moderately but, as previously mentioned, for higher speeds the silica concentrations do not increase significantly, indicating that the k-value noted for 230 rpm is probably close to a maximum. Studying particle dissolution under different physical forcing, Nienow (1985) proposed a relationship between the mass transfer coefficient and the dissipated energy by mass unit. The Nienow correlation is as follows:

$$\text{Sh} = \frac{kd_P}{D} = \left(\frac{\varepsilon^{1/3} d_P^{4/3} \rho_L}{\mu_L} \right)^{0.46} \text{Sc}^{0.33} \quad (4)$$

TABLE 3 | Calculated saturation indices (SIs) for silica mineral phases amorphous silica, chalcedony, and quartz.

Time (h)	pH	[Si] (mol L^{-1})	[H$_3$SiO$_3$] (mol L^{-1})	Saturation indices (log Q/K)		
				Quartz	Chalcedony	Amorphous silica
Rotation speed: 230 rpm						
Fresh water (MQ water)						
30	6.6	1.08E−05	4.21E−09	−0.8466	−1.1218	−2.1668
60	6.6	8.79E−06	3.42E−09	−0.9369	−1.2121	−2.2571
90	6.6	1.18E−05	4.59E−09	−0.8095	−1.0847	−2.1297
300	6.6	3.39E−05	1.32E−08	−0.3503	−0.6255	−1.6705
1440	6.6	1.23E−04	4.79E−08	0.2091	−0.0661	−1.1111
2940	6.6	2.15E−04	8.38E−08	0.4523	0.177	−0.868
4380	6.6	2.88E−04	1.12E−07	0.5791	0.3039	−0.7411
5760	6.6	3.46E−04	1.35E−07	0.6585	0.3833	−0.6617
7140	6.6	4.12E−04	1.60E−07	0.7341	0.4589	−0.5861
Seawater						
30	7.7	6.66E−06	2.96E−08	−1.0921	−1.3673	−2.4123
60	7.7	1.11E−05	4.94E−08	−0.8691	−1.1443	−2.1893
90	7.7	1.40E−05	6.22E−08	−0.7691	−1.0443	−2.0893
300	7.7	3.04E−05	1.35E−07	−0.4326	−0.7078	−1.7529
1440	7.7	6.30E−05	2.80E−07	−0.1159	−0.3911	−1.4361
2940	7.7	1.14E−04	5.05E−07	0.1401	−0.1351	−1.1801
4380	7.7	1.57E−04	6.98E−07	0.281	0.0058	−1.0393
5760	7.7	2.00E−04	8.87E−07	0.385	0.1098	−0.9353
7140	7.7	2.41E−04	1.07E−06	0.4664	0.1912	−0.8538
Rotation speed: 85 rpm						
Fresh water (MQ water)						
30	6.6	4.16E−07	1.62E−10	−2.2615	−2.5368	−3.5818
60	6.6	4.66E−07	1.82E−10	−2.2123	−2.4875	−3.5326
90	6.6	6.49E−07	2.53E−10	−2.0684	−2.3436	−3.3887
300	6.6	2.08E−06	8.10E−10	−1.5626	−1.8378	−2.8828
1440	6.6	4.61E−06	1.80E−09	−1.2171	−1.4923	−2.5373
2880	6.6	7.57E−06	2.95E−09	−1.0019	−1.2771	−2.3222
7200	6.6	1.35E−05	5.24E−09	−0.7521	−1.0273	−2.0723
9960	6.6	1.42E−05	5.52E−09	−0.7295	−1.0047	−2.0497
Seawater						
30	7.8	3.45E−07	1.89E−09	−2.3862	−2.6614	−3.7064
60	7.8	7.76E−07	4.26E−09	−2.034	−2.3092	−3.3543
90	7.8	1.26E−06	6.90E−09	−1.8239	−2.0991	−3.1441
300	7.8	3.59E−06	1.97E−08	−1.3692	−1.6444	−2.6894
1440	7.8	1.02E−05	5.58E−08	−0.9164	−1.1916	−2.2366
2880	7.8	1.47E−05	8.06E−08	−0.7568	−1.032	−2.077
7200	7.8	2.07E−05	1.13E−07	−0.608	−0.8833	−1.9283
9960	7.8	2.42E−05	1.33E−07	−0.5399	−0.8151	−1.8601
Static						
Fresh water (MQ water)						
300	6.6	1.68E−06	6.55E−10	−1.6552	−1.9304	−2.9754
1440	6.6	3.80E−06	1.48E−09	−1.3016	−1.5768	−2.6218
2880	6.6	8.62E−06	3.36E−09	−0.9452	−1.2204	−2.2654
4320	6.6	1.03E−05	4.03E−09	−0.8664	−1.1416	−2.1866
5760	6.6	1.46E−05	5.70E−09	−0.715	−0.9902	−2.0352
7080	6.6	1.49E−05	5.82E−09	−0.7062	−0.9814	−2.0265
16,080	6.6	2.15E−05	8.36E−09	−0.5489	−0.8241	−1.8691

(Continued)

TABLE 3 | Continued

Time (h)	pH	[Si] (mol L^{-1})	[H$_3$SiO$_3$] (mol L^{-1})	Saturation indices (log Q/K)		
				Quartz	Chalcedony	Amorphous silica
Seawater						
300	7.8	1.19E−06	6.52E−09	−1.8484	−2.1236	−3.1686
1440	7.8	3.28E−06	1.80E−08	−1.4085	−1.6837	−2.7287
2880	7.8	6.43E−06	3.53E−08	−1.1155	−1.3907	−2.4358
4320	7.8	9.51E−06	5.21E−08	−0.9461	−1.2213	−2.2663
5760	7.8	1.16E−05	6.37E−08	−0.8586	−1.1338	−2.1788
7080	7.8	1.25E−05	6.85E−08	−0.8269	−1.1021	−2.1471
16,080	7.8	1.90E−05	1.04E−07	−0.6454	−0.9207	−1.9657

with Sh the Sherwood number, d_p the grain diameter, D the diffusion coefficient of dissolved Si, e the dissipated energy by mass unit, Sc the Schmidt number, μ_L the liquid viscosity, and r_L the liquid density. This semi-empirical relationship links the mass-transfer coefficient to the energy of the media. While this relationship is satisfied – what we just verified for the quartz dissolution in water – the calculation of the k-value is possible.

This formulation means that for a given quartz grain diameter, the mass transfer coefficient varies with the dissipated power by mass unit according to a law in $\approx (e)^{0.15}$. This means that the system needs a very strong increase of dissipated energy to significantly modify the k-value, which is in line with our observations.

Quantitatively, the R/W ratio is expressed by the ratio $S(t)/V$ in Eq. (3), ratio between the exchanging surface area of the solid and the reactor volume. The dissolution rate is faster if there are more particles in a given volume, as shown by the initial slopes of the curves (**Figure 2**) which depend on the rock/water ratio. The characteristic time τ of the system (see **Supplementary Material** for a complete derivation of this parameter) depends only on the mass-transfer coefficient and the R/W ratio. All the experimental curves of **Figure 2C** are fitted using Eq. (6) and consequently take in into account the R/W ratio. Again, the model reproduces satisfactorily the observations.

UPSCALING TO NATURAL ENVIRONMENTS: SANDY BEACHES AND THEIR CONTRIBUTION TO THE OCEANIC SI CYCLE

Recent studies led to suspect that processes at play at the beach–ocean boundary could yield dissolved Si input to the ocean. Based on Si isotope variations, Ehlert et al. (2016) demonstrated that dissolution of lithogenic silica is likely occurring in beach sediment of the North Sea. In a lagoon near the Mediterranean Sea, Tamborski et al. (2018) established that the local DSi increase can be attributed to water drainage due to Submarine Groundwater Discharge. At mesoscopic scale, these authors also conducted *in situ* dissolution experiments of local sediment, they measured 250 μmol L^{-1} after 4 days of incubation. With grossly the same R/W (1.25 vs. 1.16) ratio our experimental

values are greater (1780 μmol L^{-1}) but their experimental device was only gentle stirred. In comparison, Anschutz et al. (2009) estimated a significantly lower Si flux in tidal sands namely 3.02 × 10^{-6} mol yr^{-1} assumed to be mediated by microbial activity. However, none of these works discussed the processes at play and more specifically the role of the waves on the dissolution rates. Here, the contribution of sandy beaches to the marine silica cycle is estimated through mass balance. The global annual Si flux (F_{Si} in Tmol yr^{-1}) resulting from the dissolution of quartz grains on sandy beaches is calculated using the same formalism as in Eq. (2). In the case of quartz dissolution in seawater this flux can be written as:

$$F_{Si} = k_{qz}(T) \times S_{qz} \times (C^*_{Si} - C^{sw}_{Si}) \qquad (5)$$

where $k_{qz}(T)$ is the temperature-dependent quartz mass transfer coefficient (m s^{-1}), S_{qz} is the grain surface of the quartz grains (m^2), C^*_{Si} is the quartz solubility (mol m^{-3}), and C^{sw}_{Si} (mol m^{-3}) is the concentration of Si in seawater. The following paragraphs discuss the assumptions related to these parameters. The values used in the mass balance calculation are summarized in **Tables 4, 5**.

(i) Reactive surface (S_{qz}): The total world coast length is 1.1 × 10^6 km (EOTP2, 2 min angle) and 31% of this length is constituted of sandy beaches (Luijendijk et al., 2018). Calculation of the average sediment volume impacted by the waves is based on the idealized surf zone represented in **Figure 4** and the numerical values of the various parameters summarized in **Tables 3–5**. V_T is the total volume of water, V_r is the volume of water devoid of sediment, and V_m is the volume containing the agitated sediment. Volumes are calculated assuming an intertidal slope (α) of 1° (Shanks et al., 2017), leading to a maximum depth e of 1.75 m at the extremity of the surf-zone (l = 100 m, **Figure 4**). The total volume of water is $V_T = l \times L \times e/2$, i.e., 1.71 × 10^{10} m^3.

The sediment is agitated by the waves only into the mixed layer close to the seafloor (in shaded brown in **Figure 4**) and the sediment concentration decreases exponentially from the bottom to the top of this layer. This mixed layer (l_m) is comprised between 0.1 and 1 m (Aagaard and Jensen, 2013); we took 0.5 m in average. Assuming that the sediment concentration decreases from the bottom (C_o) to the top of the mixing layer following an exponential law (**Figure 4**, C_o = 1 kg m^{-3}, Aagaard and Jensen, 2013; Yoon et al., 2015), we took an average sediment
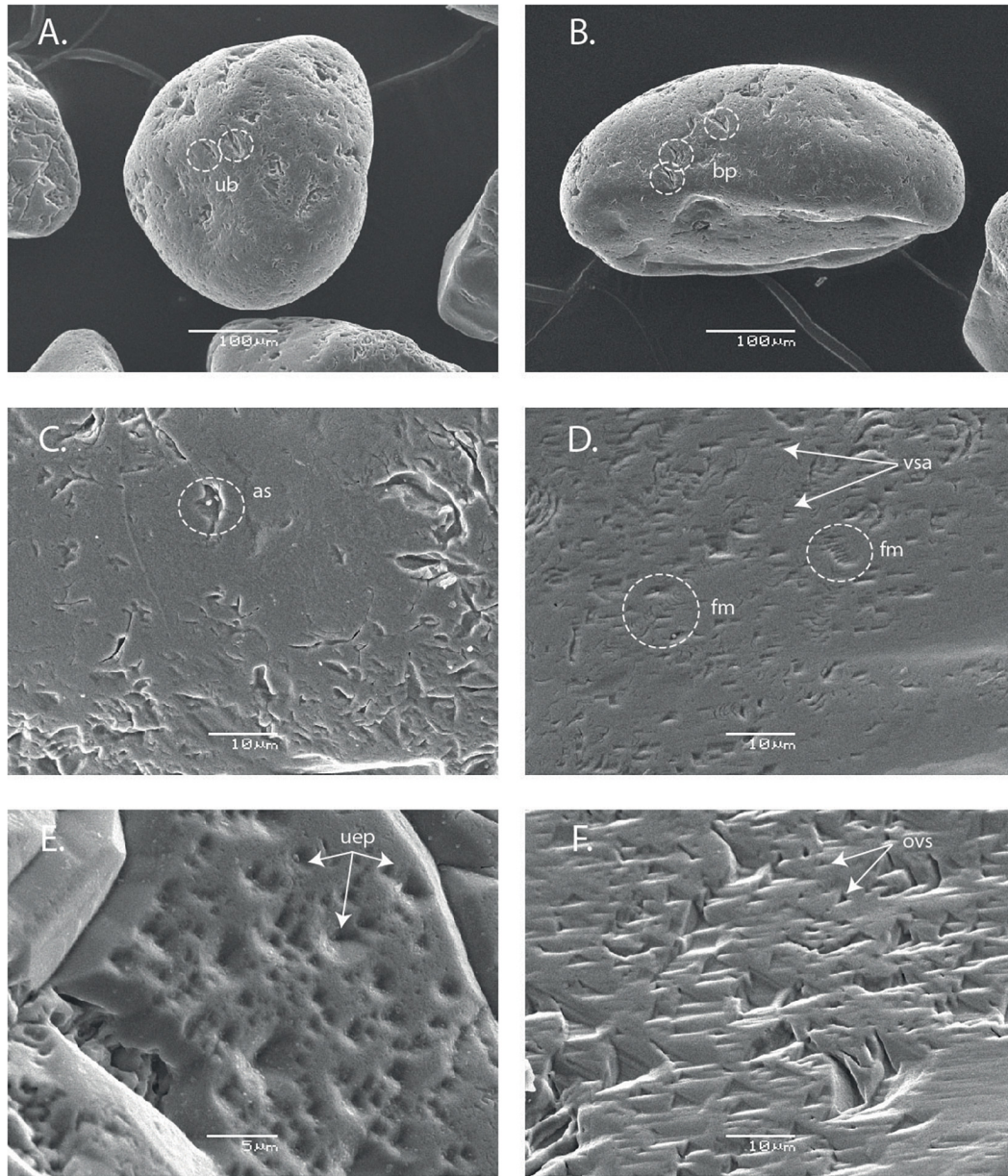
FIGURE 3 | SEM morphology of unaltered (left column) and altered (right column) sand after 10 days experiments (250 μm, R/W = 1.8). **(A)** General view of a sub-rounded quartz grain of high sphericity. It exhibits used blocky breakage conchoidal patterns (ub). **(B)** A rounded quartz grain displaying fresh blocky conchoidal patterns (fb). **(C)** Detail of a plane surface showing old arc shaped impact features (as). **(D)** High density of V-shaped abrasion (vsa) and friction marks (fm). **(E)** Detail of the upper edge of the quartz grain, used etch pits are clearly visible (uep). **(F)** Numerous oriented V-shaped patterns (ovs).

concentration of 0.42 kg m^{-3} in the mixed layer. Based on simple geometrical characteristics shown in **Figure 4**, the volume of the mixed zone is:

$$V_r = \frac{(e - l_m)^2 L}{2 tg\alpha} \tag{6}$$

and numerically $V_r = 1.58 \times 10^{10}$ m^3.

The mixed volume V_m is the difference between V_T and V_r, namely 1.28×10^9 m^3.

Finally, a compilation of diverse coastal environments gives an average sand grain size of 200 μ (Orton and Reading, 1993). Assuming spherical shape for quartz grains, the reactive surface of the sand (see Eq. 2 in the **Supplementary Material**) is $S_{qz} = 5.9 \times 10^9$ m^2.

(ii) Concentration gradient between the quartz grains and seawater: For water depths of 0–450 m, DSi values vary between ca. 5 and 70 μM, compilation established along various basin coasts (Lal, 1977). Thus, we kept a value of 35 μmol L^{-1} (or 9.8×10^{-4} kg m^{-3}) in our calculations (Eq. 5).

TABLE 4 | Parameters used for the calculation of the mass transfer coefficient.

Parameter	Symbol	Fresh water	Sea water
Density ($kg\ m^{-3}$)	ρ	1000	1024
Dynamic viscosity (Pa s)	μ	$1.0E-03$	$1.07E-03$
Kinematic viscosity ($m^2\ s^{-1}$)	$\eta = \mu/\rho$	$1.0E-06$	$1.04E-06$
Diffusion coefficient ($m^2\ s^{-1}$)	D	$1.0E-09$	$0.9E-09$
Schmidt number	Sc	400	1045

TABLE 5 | Mass transfer coefficient (k) for quartz grains in agitated solutions according to the various experimental conditions.

Solution	R/W	Speed rotation (rpm)	Mass transfer coefficient ($m\ s^{-1}$)	Sum of quadratic error* (SQE)
First set of experiments				
Seawater	1.8	0	$1.69E-11$	$1.96E-08$
		85	$3.05E-11$	$3.46E-07$
		230	$5.45E-10$	$4.60E-06$
Fresh water	1.8	0	$6.00E-12$	$6.70E-08$
		85	$9.90E-12$	$5.06E-08$
		230	$6.21E-10$	$1.40E-04$

Solution	R/W	Speed rotation (rpm)	Mass transfer coefficient ($m\ s^{-1}$)	Mean square error*
Second set of experiments				
Freshwater	5.33	230	$1.10E-09$	$4.67E-13$
	1.6	230	$5.51E-10$	$7.04E-11$
	0.78	230	$3.11E-10$	$1.77E-09$

*SQE is calculated according to the following formula: $(\Sigma(C_{calc} - C_{obs})^2)$, where C_{calc} stands for calculated concentrations, C_{obs} for observed concentrations.

C^* could be taken equal to quartz solubility (355 μmol L^{-1}), which explicitly corresponds to a system close to chemical equilibrium. However, as shown by the experimental results C^* could exceed this value – at least temporarily – up to 70% (676 μmol L^{-1}). This reflects the shaking effect, leading to a chemical disequilibrium. The final range of DSi flux calculated with Eq. (5) will reflect these two bounds. In any case, the large difference between C^* and the DSi value of the coastal waters induces a strong gradient.

(iii) Wave frequency, height, and mass-transfer coefficient: The mean height of waves and the wave frequency are taken as 1 m and 0.1 Hz, respectively (Aagaard and Jensen, 2013). The energy flux of the waves (E) depends on the wave frequency (or period T) as described by this formula

$$E = \rho g^2 H^2 T/64\pi \qquad (7)$$

where H is the significant wave height, T the wave period, ρ the water density, and g the acceleration by gravity (Svendsen, 2006). This equation expresses that the wave power is proportional to the wave period. This energy flux (E) is now converted in an energy by volume unit (ε) using the simple geometry of the shore (**Figure 4**), as required by the Nienow relationship which links the DSi flux to this energy per volume unit ($\varepsilon^{\wedge 1/3}$, i.e., 0.04 W m^{-3}). The mass transfer coefficient could then be calculated with Eq. (4), namely $k = 4.6 \times 10^{-5}$ m s^{-1} (**Table 6**). This k-value

represents the average "natural" mass transfer coefficient of DSi for sandy beaches derived from the previous assumptions (i–iii).

(iv) k_{qz} function of T: Neglecting the Antarctic continent, shore line temperatures ranges from 34 to 7°C [NOAA; NOAA Office of Satellite Production Operation, 2013]. Based on the following semi-empirical correlation between temperature and the mass transfer coefficient (Roustan, 2003):

$$k(T°C) = 1.024^{(T-20)} \times k(20°C) \qquad (8)$$

one can calculate $k(T = 7°C) = 3.4 \times 10^{-5}$ m s^{-1} and $k(T = 34°C) = 6.4 \times 10^{-5}$ m s^{-1}.

(v) Solid versus dissolved fluxes: we assume that the renewal rate of sand grains of the beach by local weathering, wind, and marine currents balance the dissolution rate and that silica concentrations in the surf zone are kept constant. This hypothesis is strengthened by the very recent Ph.D. results of G. Micolajczack (Mikolajczak Ph.D. defense on May 9, 2019) who followed the distribution of the solid discharge of the Rhône River in the Gulf of Lion for 2 years. He established that between 0 and 20 m depth on the shore, 1.6 MT yr^{-1} of sand is deposited on a surface of 10 km^2 (Mikolajczak, 2019). This sand could then be reworked on an annual scale by the currents. However, dissolving 0.1% (i.e., 0.003%, as in our seawater experiments expanded on 365 days) of this flux per year remains negligible. The resulting added DSi concentration would be circa 284 μmol m^{-3} over 1 year for the same volume. Thus, the amount of solid material annually dissolved and released to the sea is tiny compared to the flux of sediment discharged from the continent.

(vi) Final upscaling: Results are presented in **Table 6**. The calculated annual global DSi flux F_{si} ranges from 2.3 Tmol yr^{-1} (at 7°C) to 4.3 Tmol yr^{-1} (at 34.1°C) for $C^* = 355.9$ μmol L^{-1}. We kept an average value of 3.2 ± 1.0 Tmol yr^{-1}. Considering the dissolution rate induced by the wave shaking ($C^* = 676.1$ μmol L^{-1}), this average F_{si} can reach 5.0 ± 2.0 Tmol yr^{-1}. In a Mediterranean lagoon, Tamborski et al. (2018) established that the DSi flux driven by Submarine Ground Water Discharges was similar to the local river one. Using simultaneous $^{224}Ra_{ex}$ analyses, they attribute this flux to the dissolution of local sediment. Extrapolating their results to the whole length of sandy beaches discussed in this work leads to a DSi flux of 0.3 Tmol yr^{-1}. Although significant and higher than the 0.07 Tmol yr^{-1} attributed to the SGD on a global scale by Ehlert et al. (2016), this value stays 10 times lower than the 3.2 Tmol yr^{-1} derived from our study. These differences illustrate that different processes are at play in the surf zone under the wave pressure and during the discharge of Submarine Groundwaters.

Figure 5 proposes an update Tréguer and De La Rocha (2013) compilation in which the recent SGD inputs proposed by Ehlert et al. (2016) and the revised reverse weathering discussed in Rahman et al. (2017) are considered. We also added the range of DSi input flux originating from the sandy beach proposed in the present work. The new balance of DSi in the oceans is:

Sources (F^+, Tmol yr^{-1}): river DSi: 6.2 ± 1.8; river biogenic silica: 1.1 ± 0.2; submarine ground water discharge 0.07 (Ehlert et al., 2016); aeolian 0.5 ± 0.5; hydrothermal 0.6 ± 0.4; seafloor
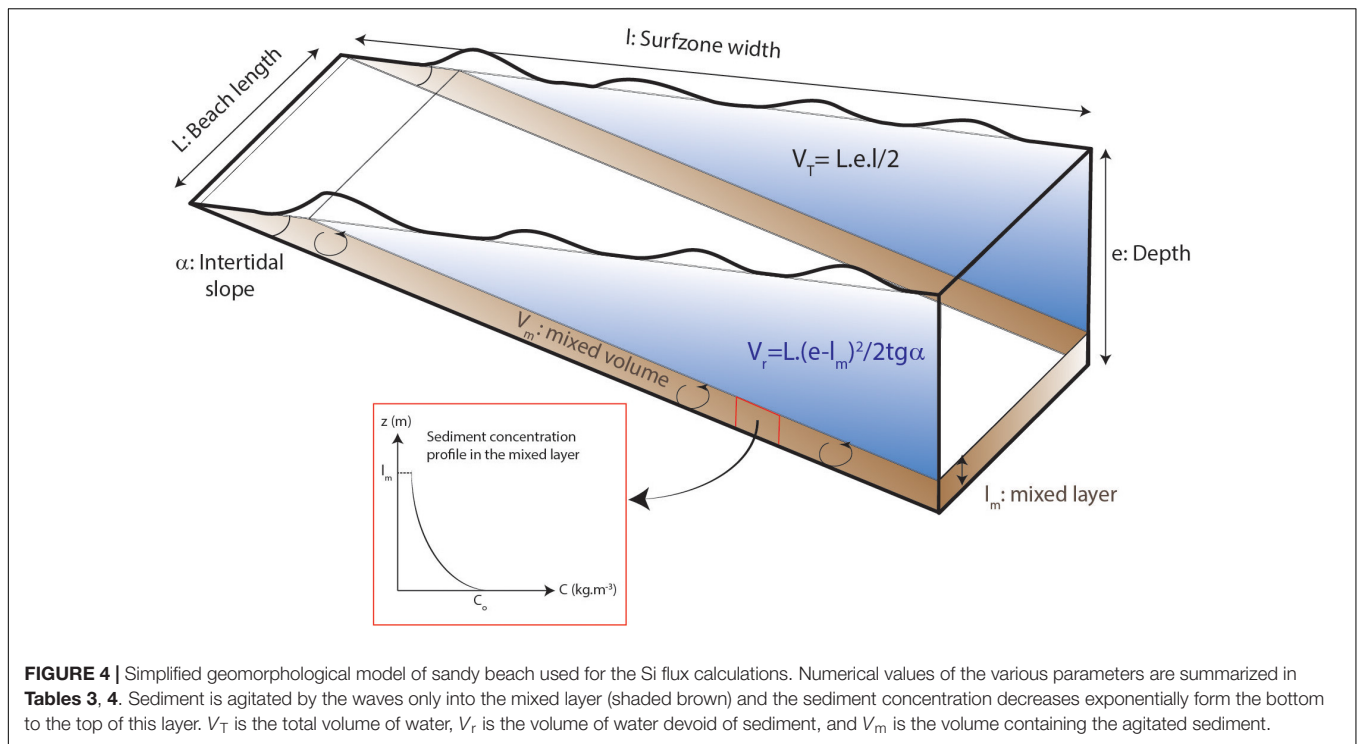
FIGURE 4 | Simplified geomorphological model of sandy beach used for the Si flux calculations. Numerical values of the various parameters are summarized in **Tables 3**, **4**. Sediment is agitated by the waves only into the mixed layer (shaded brown) and the sediment concentration decreases exponentially form the bottom to the top of this layer. V_T is the total volume of water, V_r is the volume of water devoid of sediment, and V_m is the volume containing the agitated sediment.

TABLE 6 | Calculated silica fluxes from the beach to the offshore caused by quartz grain dissolution.

Natural parameters	Symbol	Units	Value
Clastic coasts total length (ETOPO2)	L	km	3.41×10^8
Width of the mean surf beach zone	l	m	100
Mean depth 100 m from the shore (mean slope of the continental plateau of 1°)	e	m	1.75
Quartz grain density	ρ	kg m^{-3}	2700
Silica concentration in seawater	C	μmol L^{-1}	85.4
Average quartz grain diameter	d	m	2×10^{-4}
Dissipated energy for 1 m height waves	ε	W m^{-3}	4×10^{-2}
Wave frequency	N	Hz	0.1
Sediment volume agitated by the wave surf	V_m	m^3	1.28×10^9
Sediment concentration in seawater	M	kg m^{-3}	0.42
Mixed layer thickness	l_m	m	0.5
Calculations			
Mass transfer coefficient (SiO$_2$ in seawater) for 1 m height waves ($T = 20°C$)	k	m s^{-1}	4.6×10^5
Silica flux from quartz grain dissolution ($T = 20°C$)	F_{Si}	Tmol yr^{-1}	3.1
Silica flux from quartz grain dissolution ($T = 7°C$)	F_{Si}	Tmol yr^{-1}	2.3
Silica flux from quartz grain dissolution ($T = 34.1°C$)	F_{Si}	Tmol yr^{-1}	4.3

weathering: 1.9 ± 0.7; *lithogenic flux* (this study) 3.2 ± 1.0–5.0 ± 2.0 Tmol yr^{-1}, a flux comparable to the dissolved river one.

Sinks (F$^-$, Tmol yr^{-1}): reverse weathering: 4.7 ± 0.3 (Rahman et al., 2017); biological sequestration by diatoms (6.3 ± 3.6) and sponges (3.6 ± 3.7).

The last published budget was subject to large uncertainties (total sources of 10.4 ± 3.6 Tmol yr^{-1} versus total sinks of 14.6 ± 7.6 Tmol yr^{-1}). The revised one leads to a sum of sources balancing the sum of sinks (13.6 ± 4.7–15.4 ± 5.7 Tmol yr^{-1} and 14.6 ± 7.6, respectively), which is more satisfying.

BROADER IMPLICATIONS

This additional lithogenic DSi flux modifies the current vision of the global oceanic DSi cycle, notably the ratio between inputs and recycling (Tréguer and De La Rocha, 2013). The residence time at steady sate (τ_G) is equal to the total amount of DSi in the ocean (90,000 Tmol Si) divided by the sum of the net input flux (ΣF^+). The additional lithogenic flux proposed here would shorten the DSi τ_G from its present value of 10,000 to 6696 years. According to this calculation, the total oceanic DSi stock has likely been renewed twice since the beginning of the Holocene (11,500 years), strengthening the hypothesis that the oceanic DSi mass balance is at steady state. This additional flux could also impact the short carbon cycle, via the Biological Carbon Pump. Such changes in the DSi input of continental origin could also have impacted the average oceanic isotopic signature (δ^{30}Si) in the past. Glacial biogenic Si isotopic signatures (Bδ^{30}Si) measured in sediment cores are 0.5–1‰ lower than interglacial ones (Sutton et al., 2013). These authors assign 67% of the isotopic variation observed at the transition between LGM and recent ages to the modification of diatom species in response to environmental changes. We suggest here that the remaining 33% could result from changes of the δ^{30}Si of the inputs, in agreement with Frings et al. (2016). This suggestion should be taken cautiously,
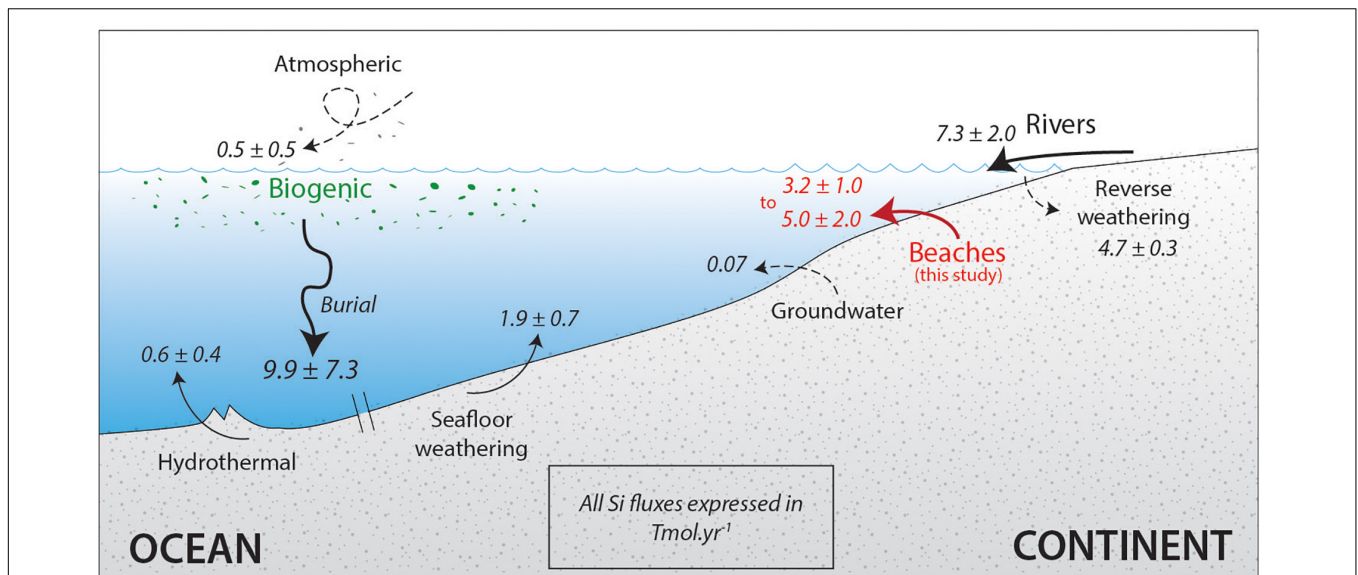
FIGURE 5 | Revised sources and sinks of the global oceanic Si cycle. Inspired by Tréguer and De La Rocha (2013). Values for reverse weathering are from Rahman et al. (2017) and for groundwater discharge from Ehlert et al. (2016).
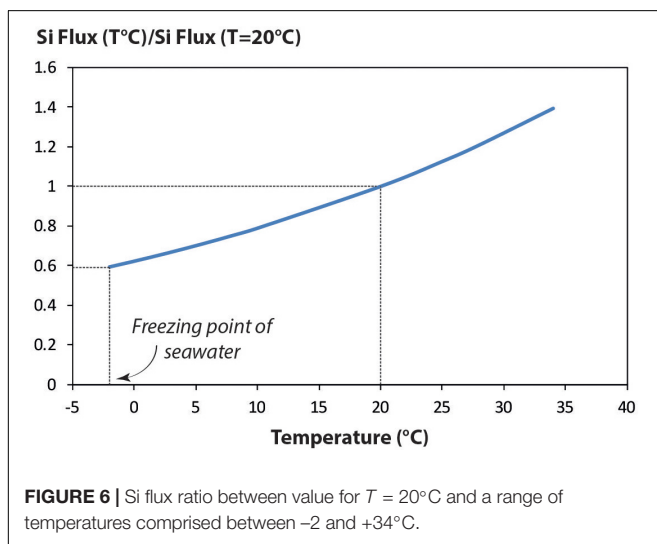

FIGURE 6 | Si flux ratio between value for $T = 20°C$ and a range of temperatures comprised between –2 and +34°C.

knowing that the variation reported by Sutton et al. (2013) was the maximum amount of variability explained by species-specific fractionation at one location. During the last glacial maximum (LGM), atmospheric CO_2 dropped from 280 to 190 ppmv likely related to an increase in surface productivity (Khatiwala et al., 2019). Indeed, several authors proposed that massive aeolian inputs of continental iron or silica during the LGM boosted the biological carbon production (Angelis et al., 1987; Duce et al., 1991; Martin et al., 1994; Monnin, 2001; Khatiwala et al., 2019). The present work also suggests that glacial conditions might have two contrasting effects for the continental Si inputs: (i) Colder oceanic waters would imply lower k_{qz}, slowing the silicate dissolution as illustrated in **Figure 6**, showing that the DSi flux would vary from −40 to +40% compared to its value at 20°C.

(ii) Contrastingly, stronger winds would have enhanced the wave energy thus the sand beach weathering (Sarnthein et al., 1981).

CONCLUSION

Laboratory experiments simulating the strong shaking due to the waves in the surf zone of the sand beaches revealed that the pure quartz dissolution kinetic was considerably accelerated.

We showed that a shrinking sphere model fitted experimental data well, suggesting that the accelerated dissolution in agitated media results from the shrinking of the *boundary layer* where the transport of aqueous species is driven by diffusion and that advection was the dominant process.

This work strongly suggests that the continuous and energetic mixing of the waves likely accelerates the dissolution kinetics of the silicates, which might yield a new DSi flux to the ocean, overlooked so far. Refining the value of this new flux with regards to the other components of the DSi oceanic cycle will require more *in situ* observations and field studies, involving concentration and isotope measurements and associated to thermodynamic and biogeochemical modeling.

DATA AVAILABILITY

The raw data supporting the conclusions of this manuscript will be made available by the authors, without undue reservation, to any qualified researcher.

AUTHOR CONTRIBUTIONS

CJ initiated the project. SF, TZ, and CJ designed and operated the experiments. SF and MR conducted the modeling calculation.

RA brought his knowledge of the surf zone dynamic. SF and CJ wrote the manuscript.

SUPPLEMENTARY MATERIAL

The Supplementary Material for this article can be found online at: https://www.frontiersin.org/articles/10.3389/feart. 2019.00231/full#supplementary-material

REFERENCES

Aagaard, T., and Jensen, S. G. (2013). Sediment concentration and vertical mixing under breaking waves. *Mar. Geol.* 336, 146–159. doi: 10.1016/j.margeo.2012.11.015

Angelis, M. D., Barkov, N. I., and Petrov, V. N. (1987). Aerosol concentrations over the last climatic cycle (160 kyr) from an Antarctic ice core. *Nature* 325, 318–321. doi: 10.1038/325318a0

Anschutz, P., Smith, T., Mouret, A., Deborde, J., Bujan, S., Poirier, D., et al. (2009). Tidal sands as biogeochemical reactors. *Estuar. Coast. Shelf Sci.* 84, 84–90. doi: 10.1016/j.ecss.2009.06.015

Arsouze, T., Dutay, J.-C., Lacan, F., and Jeandel, C. (2009). Reconstructing the Nd oceanic cycle using a coupled dynamical – biogeochemical model. *Biogeosciences* 6, 2829–2846. doi: 10.5194/bg-6-2829-2009

Banfield, J. F., Nealson, K. H., and Mineralogical Society of America, (eds) (1997). *Geomicrobiology: Interactions between Microbes and Minerals, Reviews in Mineralogy*. Washington, DC: Mineralogical Society of America.

Bennett, P. C. (1991). Quartz dissolution in organic-rich aqueous systems. *Geochim. Cosmochim. Acta* 55, 1781–1797. doi: 10.1016/0016-7037(91) 90023-X

Brady, P. V., and Walther, J. V. (1990). Kinetics of quartz dissolution at low temperatures. Chem. Geol. 82, 253–264. doi: 10.1016/0009-2541(90)90084-K

Brantley, S. L., Kubicki, J. D., and White, A. F. (2008). *Kinetics of Mineral Dissolution, in: Kinetics of Mineral Interaction*. New York, NY: Springer.

Brown, A. C., and Mclachlan, A. (2002). Sandy shore ecosystems and the threats facing them: some predictions for the year 2025. *Environ. Conserv.* 29, 62–77. doi: 10.1017/s037689290200005x

Casey, W. H. (1991). On the relative dissolution rates of some oxide and orthosilicate minerals. *J. Colloid Interface Sci.* 146, 586–589. doi: 10.1016/0021-9797(91)90225-W

Crundwell, F. K. (2014). The mechanism of dissolution of minerals in acidic and alkaline solutions: part II application of a new theory to silicates, aluminosilicates and quartz. *Hydrometallurgy* 149, 265–275. doi: 10.1016/j. hydromet.2014.07.003

De La Rocha, C. L., and Bickle, M. J. (2005). Sensitivity of silicon isotopes to whole-ocean changes in the silica cycle. *Mar. Geol.* 217, 267–282. doi: 10.1016/ j.margeo.2004.11.016

Delaney, J. M., and Wolery, T. J. (1989). The LLNL Thermochemical Database. Report UCRL- 21658. doi: 10.1016/j.margeo.2004.11.016

DeMaster, D. J. (1981). The supply and accumulation of silica in the marine environment. *Geochim. Cosmochim. Acta* 45, 1715–1732. doi: 10.1016/0016-7037(81)90006-5

Dove, P. M. (1994). The dissolution kinetics of quartz in sodium chloride solutions at 25 degrees to 300 degrees C. *Am. J. Sci.* 294, 665–712. doi: 10.2475/ajs.294. 6.665

Duce, R. A., Liss, P. S., Merrill, J. T., Atlas, E. L., Buat-Menard, P., Hicks, B. B., et al. (1991). The atmospheric input of trace species to the world ocean. *Glob. Biogeochem. Cycles* 5, 193–259. doi: 10.1029/91GB01778

Dürr, H. H., Meybeck, M., Hartmann, J., Laruelle, G. G., Roubeix, V. (2011). Global spatial distribution of natural riverine silica inputs to the coastal zone. *Biogeosciences* 8, 597–620. doi: 10.5194/bg-8-597-2011

Ehlert, C., Reckhardt, A., Greskowiak, J., Liguori, B. T. P., Böning, P., Paffrath, R., et al. (2016). Transformation of silicon in a sandy beach ecosystem: insights from stable silicon isotopes from fresh and saline groundwaters. *Chem. Geol.* 440, 207–218. doi: 10.1016/j.chemgeo.2016.07.015

Frings, P. J., Clymans, W., Fontorbe, G., De La Rocha, C. L., and Conley, D. J. (2016). The continental Si cycle and its impact on the ocean Si isotope budget. *Chem. Geol.* 425, 12–36. doi: 10.1016/j.chemgeo.2016.01.020

Gautier, J.-M., Oelkers, E. H., and Schott, J. (2001). Are quartz dissolution rates proportional to B.E.T. surface areas? *Geochim. Cosmochim. Acta.* 65, 1059–1070. doi: 10.1016/S0016-7037(00)00570-6

Gehlen, M., Malschaert, H., and Van Raaphorst, W. R. (1995). Spatial and temporal variability of benthic silica fluxes in the southeastern North Sea. *Cont. Shelf Res.* 15, 1675–1696. doi: 10.1016/0278-4343(95)00012-P

Haddad, S. C., Worden, R. H., Prior, D. J., and Smalley, P. C. (2006). Quartz cement in the fontainebleau sandstone, paris basin, france: crystallography and implications for mechanisms of cement growth. *J. Sediment. Res.* 76, 244–256. doi: 10.2110/jsr.2006.024

Hood, E. M., Sabine, C. L., and Sloyan, B. M. (2010). GO-SHIP Repeat Hydrography Manual: A collection of Expert Reports and Guidelines. IOCCP Report No. 14. doi: 10.2110/jsr.2006.024

ICDD, (1997). *PDF 40-1045. International Centre for Diffraction Data*. Newtown Square, PA: ICDD .

Jeandel, C. (2016). Overview of the mechanisms that could explain the "Boundary Exchange" at the land-ocean contact. *Philos. Trans. R. Soc. Math. Phys. Eng. Sci.* 374:20150287. doi: 10.1098/rsta.2015.0287

Jeandel, C., and Oelkers, E. H. (2015). The influence of terrigenous particulate material dissolution on ocean chemistry and global element cycles. *Chem. Geol.* 395, 50–66. doi: 10.1016/j.chemgeo.2014.12.001

Khatiwala, S., Schmittner, A., and Muglia, J. (2019). Air-sea disequilibrium enhances ocean carbon storage during glacial periods. *Sci. Adv.* 5:eaaw4981. doi: 10.1126/sciadv.aaw4981

Knauss, K. G., and Wolery, T. J. (1988). The dissolution kinetics of quartz as a function of pH and time at 70°C. *Geochim. Cosmochim. Acta* 52, 43–53. doi: 10.1016/0016-7037(88)90055-5

Krinsley, D., and Margolis, S. (1969). Section of geological sciences; a study of quartz sand grain surface textures with the scanning electron microscope. *Trans. N. Y. Acad. Sci.* 31, 457–477. doi: 10.1111/j.2164-0947.1969.tb0 2929.x

Lacan, F., and Jeandel, C. (2005). Neodymium isotopes as a new tool for quantifying exchange fluxes at the continent–ocean interface. *Earth Planet. Sci. Lett.* 232, 245–257. doi: 10.1016/j.epsl.2005.01.004

Lal, D. (1977). The oceanic microcosm of particles. *Science* 198, 997–1009. doi: 10.1126/science.198.4321.997

Luijendijk, A., Hagenaars, G., Ranasinghe, R., Baart, F., Donchyts, G., and Aarninkhof, S. (2018). The state of the world's beaches. *Sci. Rep.* 8:6641. doi: 10.1038/s41598-018-24630-6

Martin, J. H., Coale, K. H., Johnson, K. S., Fitzwater, S. E., Gordon, R. M., Tanner, S. J., et al. (1994). Testing the iron hypothesis in ecosystems of the equatorial Pacific Ocean. *Nature* 371, 123–129. doi: 10.1038/371123a0

Mikolajczak, G. (2019). *Dynamique de l'eau et des apports Particulaires Originaires du Rhône sur la marge Continentale du Golfe du Lion.* Toulouse: Toulouse III-Paul Sabatier.

Monnin, E. (2001). Atmospheric CO2 concentrations over the last glacial termination. *Science* 291, 112–114. doi: 10.1126/science.291.5501.112

Nienow, A. W. (1985). *Mixing in the Processes Industries.* London: Butterwort Heinemann.

Ning, R. Y. (2003). Discussion of silica speciation, fouling, control and maximum reduction. *Desalination* 151, 67–73. doi: 10.1016/S0011-9164(02)00973-6

NOAA Office of Satelllite Production Operation (2013). *Sea Surface Temperature (SST) Contour Charts [WWW Document], 2013.* Available at: http://www.ospo.noaa.gov/Products/ocean/sst/contour/ (accessed June 19, 2013).

Orton, G. J., and Reading, H. G. (1993). Variability of deltaic processes in terms of sediment supply, with particular emphasis on grain size. *Sedimentology* 40, 475–512. doi: 10.1111/j.1365-3091.1993.tb01347.x

Parkhurst, D., and Appelo, C. A. J. (1999). *User's guide to PHREEQC (version 2) - a Computer Program For Speciation, Batch-Reaction, One-Dimensional Transport, And Inverse Geochemical Calculations, Water-Ressources Investigations Report 99-4259.* Colorado.

Ragueneau, O., Schultes, S., Bidle, K., Claquin, P., and Moriceau, B. (2006). Si and C interactions in the world ocean: importance of ecological processes and implications for the role of diatoms in the biological pump. *Glob. Biogeochem. Cycles* 20:GB4S02. doi: 10.1029/2006GB002688

Ragueneau, O., Tréguer, P., Leynaert, A., Anderson, R. F., Brzezinski, M. A., DeMaster, D. J., et al. (2000). A review of the Si cycle in the modern ocean: recent progress and missing gaps in the application of biogenic opal as a paleoproductivity proxy. *Glob. Planet. Change* 26, 317–365. doi: 10.1016/S0921-8181(00)00052-7

Rahman, S., Aller, R. C., and Cochran, J. K. (2017). The missing silica sink: revisiting the marine sedimentary Si cycle using cosmogenic 32 Si: the missing sedimentary silica sink. *Glob. Biogeochem. Cycles* 31, 1559–1578. doi: 10.1002/2017GB005746

Rahman, S., Tamborski, J. J., Charette, M. A., and Cochran, J. K. (2019). Dissolved silica in the subterranean estuary and the impact of submarine groundwater discharge on the global marine silica budget. *Mar. Chem.* 208, 29–42. doi: 10.1016/j.marchem.2018.11.006

Roustan, M. (2003). *Transferts Gaz-Liquide Dans Les Procédés De Traitement Des Eaux Et Des Effluents Gazeux.* Paris: Tech & doc.

Sarnthein, M., Tetzlaff, G., Koopmann, B., Wolter, K., and Pflaumann, U. (1981). Glacial and interglacial wind regimes over the eastern subtropical Atlantic and North-West Africa. *Nature* 293, 193–196. doi: 10.1038/293193a0

Shanks, A. L., Morgan, S. G., MacMahan, J., and Reniers, A. J. H. M. (2017). Alongshore variation in barnacle populations is determined by surf zone hydrodynamics. *Ecol. Monogr.* 87, 508–532. doi: 10.1002/ecm.1265

Strickland, J. D., and Parsons, T. R. (1972). *A Practical Handbook Of Seawater Analysis.* Ottawa, ON: Fisheries Reasearch Board of Canada.

Sutton, J. N., Varela, D. E., Brzezinski, M. A., and Beucher, C. P. (2013). Species-dependent silicon isotope fractionation by marine diatoms. *Geochim. Cosmochim. Acta* 104, 300–309. doi: 10.1016/j.gca.2012.10.057

Svendsen, I. A. (2006). *Introduction to Nearshore Hydrodynamics, Advanced Series On Ocean Engineering.* Singapore: World Scientific.

Tamborski, J., Bejannin, S., Garcia-Orellana, J., Souhaut, M., Charbonnier, C., Anschutz, P., et al. (2018). A comparison between water circulation and terrestrially-driven dissolved silica fluxes to the Mediterranean Sea traced using radium isotopes. *Geochim. Cosmochim. Acta.* 238, 496–515. doi: 10.1016/j.gca.2018.07.022

Tréguer, P. J., and De La Rocha, C. L. (2013). the world ocean silica cycle. *Annu. Rev. Mar. Sci.* 5, 477–501. doi: 10.1146/annurev-marine-121211-172346

Van Cappellen, P. (1996). Reactive surface area control of the dissolution kinetics of biogenic silica in deep-sea sediments. *Chem. Geol.* 132, 125–130. doi: 10.1016/S0009-2541(96)00047-2

Van Cappellen, P., and Qiu, L. (1997). Biogenic silica dissolution in sediments of the Southern Ocean. I. solubility. *Deep Sea Res. Part II Top. Stud. Oceanogr.* 44, 1109–1128. doi: 10.1016/S0967-0645(96)00113-0

Vos, K., Vandenberghe, N., and Elsen, J. (2014). Surface textural analysis of quartz grains by scanning electron microscopy (SEM): from sample preparation to environmental interpretation. *Earth-Sci. Rev.* 128, 93–104. doi: 10.1016/j.earscirev.2013.10.013

Yoon, H.-D., Cox, D., and Mori, N. (2015). Parameterization of time-averaged suspended sediment concentration in the nearshore. *Water* 7, 6228–6243. doi: 10.3390/w7116228